

A new class of discontinuous solar wind solutions

Bidzina M. Shergelashvili,^{1,2,3*} Velentin N. Melnik,⁴ Grigol Dididze,^{2,3,5}
 Horst Fichtner,⁶ Günter Brenn,⁷ Stefaan Poedts,^{5,8} Holger Foysi,⁹
 Maxim L. Khodachenko,^{1,10,11} and Teimuraz V. Zaqarashvili^{12,13,3}

¹Space Research Institute, Austrian Academy of Sciences, Schmiedlstrasse 6, 8042 Graz, Austria

²Centre for Computational Helio Studies at Faculty of Natural Sciences and Medicine, Ilia State University, Cholokashvili Ave. 3/5, 0162 Tbilisi, Georgia

³Evgeni Kharadze Georgian National Astrophysical Observatory, Abastumani, 0301 Adigeni Municipality, Georgia

⁴Institute of Radio Astronomy, National Academy of Sciences of Ukraine, Kharkov, Ukraine

⁵Centre for mathematical Plasma Astrophysics, KU Leuven, Celestijnenlaan 200 B, B-3001, Leuven, Belgium

⁶Institut für Theoretische Physik IV, Plasma-Astroteilchenphysik, Universitätsstraße 150, 44801 Bochum, Germany

⁷Institute of Fluid Mechanics and Heat Transfer, Graz University of Technology, 8010 Graz, Austria

⁸Institute of Physics, University of Maria Curie-Skłodowska, PL-20-031 Lublin, Poland

⁹Institut für Fluid- und Thermodynamik, Universität Siegen, Paul-Bonatz-Str. 9-11, 57068 Siegen, Germany

¹⁰Skobel'syn Institute of Nuclear Physics, Moscow State University, Moscow, Russia

¹¹Institute of Laser Physics, SB RAS, Novosibirsk 630090, Russia

¹²Institute of Physics, IGAM, University of Graz, Universitätsplatz 5, 8010 Graz, Austria

¹³Faculty of Natural Sciences and Medicine, Ilia State University, Cholokashvili Ave. 3/5, 0162 Tbilisi, Georgia

Accepted XXX. Received YYY; in original form ZZZ

ABSTRACT

A new class of one-dimensional solar wind models is developed within the general polytropic, single-fluid hydrodynamic framework. The particular case of quasi-adiabatic radial expansion with a localized heating source is considered. We consider analytical solutions with continuous Mach number over the entire radial domain while allowing for jumps in the flow velocity, density, and temperature, provided that there exists an external source of energy in the vicinity of the critical point which supports such jumps in physical quantities. This is substantially distinct from both the standard Parker solar wind model and the original nozzle solutions, where such discontinuous solutions are not permissible. We obtain novel sample analytic solutions of the governing equations corresponding to both slow and fast wind.

Key words: Sun: corona – solar wind – methods: analytical – numerical

1 INTRODUCTION

The modeling of the quasi-stationary patterns of the solar wind flows originated from the pioneering work of Eugene Parker establishing the concept of the solar wind (Parker 1958d) and its applications to its interaction with the terrestrial magnetosphere (Parker 1958a), to magnetic field instabilities (Parker 1958b), to cosmic ray modulation (Parker 1958c, 1965b), and to shocks (Parker 1959a,b). The fundamental importance of such studies for our understanding of the physics of the Sun, its planetary system and the entire heliosphere has been proven during the past six decades by numerous investigations. There is a particular need to investigate the basic mechanisms that drive the dynamics and

thermodynamics of the solar atmosphere and the wind outflow into the interplanetary space, thus shaping the whole heliosphere. The vast progress made in both analytical and numerical modelling (see, e.g., the reviews Tsinganos 2007; Cranmer & Winebarger 2019) has been accompanied by an extensive collection of observational data from a wide variety of space and ground based missions. Currently, state-of-the-art solar and space condition monitoring infrastructures exist (via the spacecraft ACE, SDO, Parker Solar Probe etc.) as well as data-driven prediction and research models, like AWSoM (van der Holst et al. 2014), ENLIL (Odstrcil 2003), or EUFORIA (Pomoell & Poedts 2018).

As such, modern space weather research infrastructures consist of combinations of many analytical, numerical and observational methodologies that complement each other. The mutual development of these three types of approaches is one of the main challenges, motivated by the need for a

* E-mail: bidzina.shergelashvili@oeaw.ac.at or bidzina.shergelashvili@iliauni.edu.ge

deeper insight in the physical mechanisms behind the solar/space weather, planetary and/or heliospheric physics. The content of the present paper falls in this framework and represents an attempt to contribute to the described challenges. We refer the interested reader to the well-structured reviews on the nature of the solar wind sources in the corona/solar atmosphere (Feldman et al. 2005) and solar wind interplanetary patterns (Echim et al. 2011), and references therein.

One of the important aspects in space weather is the physical state of the solar corona and of the inner solar atmosphere where the physical driving processes of different flow patterns are located. The identification and classification of these sources is possible through remote observations of the processes in the vicinity of the Sun (e.g., electromagnetic waves in the radio range) and in-situ data at the Lagrangian (L1) point, in combination with analytical and numerical models as conceptual ground for interpretation and analysis of these data.

In the present paper, we consider a one-dimensional stationary model for the radial profiles of the physical quantities in the non-isothermal, quasi-polytropic solar wind patterns. We derive a class of solutions that are obtained from the hydrodynamic 1D model of the Solar Wind (SW) where polytropic relations between the pressure, density and temperature hold (Jacobs & Poedts 2011) outside of discontinuities. The single-fluid description is chosen to reveal the core of the physical nature of the new solutions and their behaviour at the critical point. We address the crucial issue of 'integration constants' that represent (dynamic) invariants of the profile combinations. The formalism follows the same philosophy as the standard Parker's wind mode, i.e. both the isothermal one (Parker 1958d) or the later model including the effect of the thermal conduction (Parker 1965a).

In spite of the fact that the novel solutions are derived within a general polytropic framework, we discuss throughout this paper the particular case of adiabatic systems where there is no exchange of heat between the flowing fluid elements and the environment and any changes of the internal energy of the plasma occur only at the expense of the work done by a plasma parcel on its surroundings or vice versa.

We emphasise that the model presented here is stationary and purely radial. The latter condition implies that, similarly to the standard Parker's hydrodynamic SW model, it is assumed that the flow profile is formed along an irrotational, spherically symmetric radial magnetic field with the consequence that the influence of the Lorentz force on the plasma flow is excluded. Such 1D models mimic only roughly the complete patterns of the SW flow from the Sun to 1 AU and beyond. However, their physical precision is acceptable within the altitude ranges where the magnetic and flow fields rotate rigidly, i.e. the region with $r < 0.1$ AU, which is the subject of main interest here. Nevertheless, one must be aware that such hydrodynamic descriptions are used as a first approximation of the shape and dynamics of the inner heliosphere.

Following a description of the model in section 2, we give an interpretation of the transsonic solutions in section 3 with an emphasis on a new class of solutions, give examples for the latter, and discuss the required physical conditions. Finally, in section 4 we summarize the results and draw conclusions.

2 DESCRIPTION OF THE MODEL

The model is based on the following equations:

$$\frac{\partial \rho}{\partial t} + \nabla \cdot \rho \mathbf{v} = 0, \quad (1)$$

$$\rho \left[\frac{\partial \mathbf{v}}{\partial t} + (\mathbf{v} \cdot \nabla) \mathbf{v} \right] = -\nabla p - \rho \frac{GM_{\odot}}{r^2} \cdot \mathbf{n}_r, \quad (2)$$

where, ρ , p , \mathbf{v} , and \mathbf{B} denote the plasma mass density, (thermal) pressure, velocity, respectively. G is the gravitational constant, M_{\odot} the mass of the Sun, and \mathbf{n}_r a radial unit vector. Furthermore, we consider the energy equation of a polytropic gas flow, which is valid for the case of isentropic (adiabatic) flow patterns and, along with the ideal gas law, closes the system of the governing equations:

$$\left[\frac{\partial}{\partial t} + (\mathbf{v} \cdot \nabla) \right] \left(\frac{T}{\rho^{\alpha-1}} \right) = 0. \quad (3)$$

with α denoting the polytropic index (we will consider here the case where $\alpha = \gamma$, where γ is the adiabatic index). In general, on the r.h.s. of this equation source terms appear, encompassing the heat (entropy) production or transport that can maintain the irreversible polytropic motion of plasma elements. Here, however, we limit the study to adiabatic processes, with the aim to reveal fundamental properties of the new class of stationary solutions for the flow patterns.

For the case of purely radial but non-isothermal and stationary outflow (possibly along a global radial magnetic field, so that the Lorentz force vanishes) one has:

$$r^2 \rho v = Q_{\rho} = \text{const}, \quad (4)$$

$$v \frac{dv}{dr} = -\frac{1}{\rho} \frac{dp}{dr} - \frac{GM_{\odot}}{r^2}, \quad (5)$$

$$\frac{d}{dr} \frac{T}{\rho^{\alpha-1}} = 0, \quad (6)$$

where, similarly to the standard isothermal Parker solar wind outflow, the radial mass flow rate Q_{ρ} is an integration constant determined by the boundary condition at a given location along the radius (in standard cases it is used to satisfy values of the density and flow velocity at 1 AU or at the so-called source surface, where the wind is assumed to be purely radial). v denotes the radial component of the velocity, $\rho = \mu m_p n$ is the plasma mass density with the mean molecular weight μm_p (where μ is the mean molecular mass in units of the proton mass m_p and n is the plasma number density). Conveniently, the ideal gas law holds for the considered flow patterns $p = nk_B T$, where k_B is the Boltzmann constant. With the ideal gas law one obtains from Eqs. (5) and (6):

$$v \frac{dv}{dr} = -C_s^2 \frac{1}{\rho} \frac{d\rho}{dr} - \frac{GM_{\odot}}{r^2}, \quad (7)$$

where,

$$C_s^2 = \left(\frac{\partial p}{\partial \rho} \right)_s = \frac{\alpha k_B T}{\mu m_p} \quad (8)$$

is the square of the sound speed. Further, using Eq. (4) we derive a differential equation for a single unknown in a similar manner as in Summers (1982) for the two fluid polytropic

wind or for the classical Parker wind (see, e.g. Parker 1958d; Mann et al. 1999):

$$\frac{r}{v} \frac{dv}{dr} = \frac{2C_s^2 - \frac{GM_\odot}{r}}{v^2 - C_s^2}. \quad (9)$$

This equation implies the existence of (a) critical (singular) point(s) in the solution and determines its (their) position:

$$r = r_c = \frac{GM_\odot}{2C_s^2} = R_\odot \frac{V_{\odot,esc}^2}{4C_s^2}, \quad (10)$$

where, the Mach number $M = v/C_s$ with $V_{\odot,esc}^2 = 2GM_\odot/R_\odot$ being the squared gravitational escape velocity at the solar surface. The family of these transonic solutions is very well documented in the related literature and, therefore, we will not repeat their analysis here. We just address several fundamental aspects related to the construction of an additional class of solutions in the following section.

3 A NEW CLASS OF TRANSONIC SOLUTIONS

3.1 Mathematical conditions

Recall that the theory of stellar winds developed by Eugene Parker was the realization of the concept that radial variability of the gravitational force and other physical quantities imposes an analogy with industrial hydrodynamic sub- and supersonic nozzles and diffusers, and Eq. (9) provides the mathematical background for this analogy. In the isothermal SW model (i.e. with the polytropic index $\alpha = 1$), the solution space is constructed with the requirement that the nominator and the denominator on the r.h.s. of Eq.(9) both vanish at a critical point. This requirement permits finite values for the spatial velocity derivative at the critical point. However, one has to notice that even when the singularity is removed, the presence of the bifurcation point implies ‘a physical/configurational singularity’ manifested in the fact that an observer to the right of the critical point in the $v-r$ plane may not realize to which kind of flow pattern (sub- or supersonic) this point belongs to, and for a clear conclusion it is needed to move at least by an infinitesimal distance in the left or right direction from this point (enabling a conclusion about the sign of the gradient in this point). As a matter of fact, this ambiguity shows that sub- and supersonic parts of the flow can represent formally mutually independent patterns, and the position of the critical point for each of them can be uniquely determined by the corresponding boundary conditions, viz. on the left side from the critical point these conditions are set at the base of the corona (boundary value problem) and for the right side usually the physical quantities at infinity define the position of the critical point.

The fact that, within the considered set up, the integration constants in the corresponding governing equations are chosen in a way that the positions of the critical point derived from the left and right sides coincide, does not remove the physical independence of these parts of the flow pattern. This independence becomes evident if we recall the analogy with the interconnected hydrodynamic sub- and supersonic nozzles. As a matter of fact, it is well known that in the subsonic nozzle the maximum Mach number that could be achieved is $M = 1$. The same is valid for the supersonic

nozzle with the difference that the value $M = 1$ represents a global minimum in this case and it can not be dropped below this value.

It is important to note that in this case, if one demands that

$$1 - \frac{GM_\odot}{2C_{s1}^2 r_*} = 1 - \frac{GM_\odot}{2C_{s2}^2 r_*} = 0, \quad (11)$$

then in the critical point the nominator in Eq.(9) vanishes. This set of conditions restricts significantly the space of available solutions as it dictates that the governing equations must be solved subject to the just outlined conditions. It is easy to show that in such case all the solutions are smooth and for $\alpha > 3/2$ only decelerating from supersonic to subsonic states exist. The threshold value $3/2$ is known as the Parker polytrope, see e.g. Tsinganos (1996).

However, in general terms, the discontinuous solution is not forbidden, i.e. we can have a wider class of solutions for the SW flow patterns. In general, the restriction of smooth transonic outflow can be dropped and the nominator and denominator of the r.h.s. of Eq. (9) can vanish at different points. In this case the position of the singularity is determined entirely by the condition $M = 1$, which implies infinite radial gradients in velocity, density, and temperature. In other words, subject of our paper is to explore the extension of the solution space when the mentioned restrictions are absent, implying that there is some physical process in the singular jump region enabling and

$$1 - \frac{GM_\odot}{2C_{s1}^2 r_*} \neq 1 - \frac{GM_\odot}{2C_{s2}^2 r_*} \neq 0, \quad (12)$$

at the critical point.

This way a wider class of solutions can be constructed by setting boundary conditions accordingly, provided that the second law of thermodynamics is respected and the entropy increases across the jump.

In order to continue the description of our formalism, it is convenient to introduce an auxiliary function $r_c(r)$:

$$r_c(r) = \frac{GM_\odot}{2C_s^2(r)}. \quad (13)$$

This function defines the position of the point $r_0 = r_c(r_0)$ where the nominator of the r.h.s. of Eq. (9) vanishes. In case the condition (11) holds, we have a standard transonic smooth solution when the points r_{01} and r_{02} corresponding to the ‘upstream’ and ‘downstream’ states satisfy the relation $r_{01} = r_{02} = r_*$. Otherwise, these points differ from each other and a jump can be formed at the critical point r_* .

In summary, the solutions for flow patterns that could be covered by (9) are of two kinds: (i) when the mentioned two points are placed at the same radial distance to maintain the existence of a finite flow velocity derivative everywhere within the radial domain; (ii) When these two points are different and singular jumps in physical quantities appear.

Further, by denoting $\eta = r/r_c$ as a dimensionless distance variable and $\xi = M^2$ and using the obvious relation

$$\frac{d \ln r_c}{dr} = -\frac{d \ln C_s^2}{dr}, \quad (14)$$

it is straightforward to prove that the following equation is valid:

$$(5 - 3\alpha) \frac{d \ln C_s^2}{dr} + (\alpha - 1) \left(\frac{d \ln \xi}{dr} + 4 \frac{d \ln \eta}{dr} \right) = 0, \quad (15)$$

from which it becomes evident that in the limit $\alpha \rightarrow 1$ the formalism developed here reduces to the Parker's thermodynamically isothermal wind, and in the particular case of considered in this paper it reduces to the constant temperature case (see, e.g. [Mann et al. 1999](#)) as we omit thermal conduction and/or other transport processes.

In order to perform a thorough analysis of the developed analytical framework, it is convenient to present (9) in terms of η and ξ :

$$\frac{d\xi}{dr} - \frac{d \ln \xi \eta^4}{dr} - (3 + \xi) \frac{d \ln r_c}{dr} = -\frac{4r_c}{r^2}, \quad (16)$$

which represents a most general equation generating the space of flow pattern solutions in combination with Eq. (15) and the boundary conditions for the density, flow velocity and temperature being in accordance with the above stated jump conditions. In case of existence of a critical point above the stellar surface, the boundary conditions are to be selected separately upstream and downstream w.r.t. the critical point.

3.2 Flow patterns of monatomic adiabatic gas

$$\alpha = \gamma = 5/3$$

It is well known from the thermodynamics that monatomic gases with intrinsic particle motions with three degrees of freedom have the adiabatic index equal to $5/3$ (as a fraction of the specific heat capacities c_p/c_v). As noted above, we limit the study to adiabatic processes outside the discontinuity to reveal the properties of the new class of solutions in a most simple set-up. The adiabaticity implies the absence of any means for entropy generation or its microscopic transport above the solar surface. All sources maintain the thermodynamic state at the so-called source surface, and the only process is the macroscopic convective transport by the flow with velocity v under the action of the gravitational force and the thermal pressure gradient. For $\alpha = 5/3$, the first term in the Eq. (15) vanishes and, as $\alpha \neq 1$, the solution of the equation is:

$$\xi \eta^4 = C_*^2 = \text{const}, \quad (17)$$

where C_* is a dimensionless integration constant (for convenience, in the further discussion it is introduced in the squared form). It is straightforward to show that, in case of $\alpha = 5/3$,

$$C_* = \frac{16Q_\rho Q_{C_s}^{3/2}}{R_\odot^2 V_{esc}^4}, \quad (18)$$

where

$$Q_{C_s} = \frac{C_s^2}{\rho^{2/3}} = \text{const}, \quad (19)$$

is another constant of integration, representing the specific entropy, and Eq. (16) takes the form

$$\frac{d\xi}{dr} - (3 + \xi) \frac{d \ln r_c}{dr} = -\frac{4r_c}{r^2}, \quad (20)$$

which governs the stationary adiabatic (isentropic) 1D flow. Notice the substantial difference compared to its equivalent and well-known isothermal counterpart: the term with a derivative of $\ln \xi$ is absent, which drastically changes the immanent physics of the flow process!

In the isothermal case ($\alpha = 1$), the condition (17) does not have to be satisfied and, thus, the corresponding equation includes the term with the derivative of $\ln \xi$ and, as a result, admits a transonic solution which passes through the critical point $(\xi, \eta) = (1, 1)$. This solution corresponds to the solution where both the nominator and the denominator of the Eq. (9) are equal to zero (simultaneously). The latter is achieved by the corresponding choice of the integration constant in the equation, which physically means setting the specific boundary conditions of the pressure and other quantities that maintain the desirable solution (when the Mach number becomes $= 1$ in a single critical point coinciding with the one where the escape velocity and the sound speed values yield a vanishing nominator in Eq. (9)). In the case of constant temperature ([Mann et al. 1999](#)) r_c is by definition a constant and η thus represents just the radial distance normalized by the critical one. In the case of adiabatic expansion of the gas with $\alpha = 5/3$, the existence of similar solution, with nominator and denominator simultaneously vanishing, requires $C_* = 1$, which again fixes the specific values of the physical quantities via Eq. (18). It is easy to show that, contrary to the isothermal case, now the selected solution is valid only for the pattern for which both $\xi \equiv 1$ and $\eta \equiv 1$ throughout of their entire domain of definition (arbitrary r).

This situation can be interpreted as follows: if the specific entropy and the mass flow rate on the source surface and at infinity coincide, then there is no transonic solution available as the Mach number $M = 1$ everywhere. The solution for the sound speed and flow velocity, in this case, can be written as:

$$v(r) = C_s(r) = \left(\frac{GM_\odot}{2r} \right)^{1/2}. \quad (21)$$

The difference to the classic Parker's case becomes clear if we recall that the motion of each fluid element along the streamlines in the isothermal case is supported by some process of microscopic transport or generation of entropy. In the adiabatic case, there are no such transport processes (for instance, thermal conduction) or sources available. The specific volume deformation of the fluid elements along their trajectories is done entirely at the expense of internal energy, and the radial profiles of density, temperature and velocity are solely determined by the macroscopic convective transport with the velocity field $v(r)$.

In order to have a single critical point in the non-isothermal cases, the non-adiabatic (non-equilibrium) sources of the entropy production or transport must be at work. At microscopic scales perhaps one of the good candidates again is thermal conduction, while macroscopic MHD turbulence (e.g. see [Vainio et al. 2003](#); [Shergelashvili & Fichtner 2012](#), and references therein) or other wave processes in non-equilibrium media ([Shergelashvili et al. 2007, 2006](#)) can provide a substantial contribution into the solar wind pattern formation. The nonadiabatic framework of the problem is beyond the scope of the present study. Here, we just underline one important aspect of the given comparison, namely that for both the isothermal and the adiabatic cases, for the existence of a critical point, the nominator and denominator of the Eq. (9) have to vanish simultaneously. In order to achieve this, one has to set specific values of the physical quantities at the boundaries. Such selection

is similar to maintaining a so-called design pressure for the engineering realization of a subsonic-supersonic nozzle. It is plausible to assume that apart from these solution patterns satisfying the specifically tuned 'design pressure' conditions, there exists a wider class of flow solutions admitting finite nonzero values of the nominator in Eq. (9) at the critical point ($M = 1$) and as a result including the cases of the flows which have jumps (discontinuous behaviour) of the physical quantities at that point. All those solutions are obtained through an arbitrary choice of the values of the integration constant from the domain $C_* \neq 1$.

Let us consider this more general class of solutions for the case of $\alpha = 5/3$. By substitution of the Eq. (17) into Eq. (16) one obtains:

$$\frac{d}{dr} \left[\ln \frac{\eta(3 + C_*^2 \eta^{-4}) - 4}{r} \right] = 0, \quad (22)$$

which translates into the algebraic quartic equation for η

$$3\eta^4 - (4 + Dr)\eta^3 + C_*^2 = 0, \quad (23)$$

where D is the third integration constant, the physical nature of which will be revealed in the following discussion. Applying the Ferrari-Cardano theory of quartic equations, the general solution of this equation can be written in the form:

$$\begin{aligned} \eta_{1,2} &= -\frac{b}{2a} - S \pm \frac{1}{2} \left(-4S^2 - \frac{P}{4a^2} + \frac{b^3}{8a^3S} \right)^{\frac{1}{2}} \\ \eta_{3,4} &= -\frac{b}{2a} + S \pm \frac{1}{2} \left(-4S^2 - \frac{P}{4a^2} - \frac{b^3}{8a^3S} \right)^{\frac{1}{2}}, \end{aligned} \quad (24)$$

where

$$\begin{aligned} S &= \frac{1}{2} \left(-\frac{P}{12a^2} + \frac{1}{3a} \left(H + \frac{\Delta_0}{H} \right) \right)^{\frac{1}{2}} \\ P &= -3b^2, \end{aligned} \quad (25)$$

and:

$$\begin{aligned} \Delta_0 &= 12ae \\ H &= \left(\frac{\Delta_1 + (\Delta_1^2 - 4\Delta_0^3)^{\frac{1}{2}}}{2} \right)^{\frac{1}{3}}. \end{aligned} \quad (26)$$

Here, $a = 3$, $b = -(4 + Dr)$ and $e = C_*^2$, $\Delta_1 = 27b^2e$. It is also convenient to introduce the additional parameters

$$\begin{aligned} \Delta &= (4\Delta_0^3 - \Delta_1^2) / 27 = 256a^3e^3 - 27b^4e^2 = 27C_*^4(256C_*^2 - b^4) \\ K &= 64a^3e - 3b^4 = 3(576C_*^2 - b^4). \end{aligned} \quad (27)$$

Our goal is to investigate classes of solutions that give real η values along the considered radial domain $r/R_\odot > 1$.

It is evident that $P < 0$. Besides, if $\Delta > 0$, then $K > 0$ (these relations forbid in the considered case the solution with four distinct real solutions for any r). In general, these conditions significantly restrict the set of available real solutions. To obtain the flow patterns, the equation has to be evaluated in each r , which is subject to the boundary conditions that determine the constants D and C_* . For the further analysis it is appropriate to distinguish the following cases: (i) when $\Delta < 0$, then two out of four solutions (24) are real and distinct; (ii) when $\Delta = 0$, then multiple roots may exist. In particular, if $P < 0$, $K < 0$, and $\Delta_0 \neq 0$ there are one double and two simple real roots, when $K > 0$ there

exists one double real root, and if $\Delta_0 = 0$ and $K \neq 0$ there are one triple and one simple root, all real.

We continue the analysis with the latter case from (ii) which corresponds to $\Delta_0 = 36C_*^2 = 0$ i.e. $C_* = 0$ and, thus, no flow according to definition (18) that implies $Q_\rho = r^2\rho v = 0$. Then, Eq.(23), as expected, has one physically meaningless triple solution $\eta = 0$ and one nontrivial solution:

$$\eta = \frac{4 + Dr}{3}, \quad (28)$$

where the constant $D \geq -4/R_\odot$ can be chosen arbitrarily to give the solution for the temperature and density profiles in the stationary streamlines:

$$C_s^2 = Q_{C_s} \rho^{\frac{2}{3}} = \frac{GM_\odot D}{6} \left(1 + \frac{4}{Dr} \right) = \frac{V_{\odot esc}^2 DR_\odot}{12} \left(1 + \frac{4}{Dr} \right), \quad (29)$$

provided that $D > 0$ as both temperature and density must be positive everywhere.

It should be noted that if the solution contains a critical point where the $M = 1$, then the subsonic and supersonic parts of the flow have to be considered as two interconnected states and the boundary conditions are set such that these two states are matched in the common critical point $r = r_*$ where both states maintain $M = 1$, that enabling a 'smooth' transition on the (ξ, η) plane. The existence of such critical point requires that the corresponding root $\eta = \eta_*$ has to be double which corresponds again to the case (ii): $\Delta = 0$ with $\Delta_0 \neq 0$, which is equivalent to $C_* \neq 0$ and a finite flow velocity. Then it is easy to check that $K > 0$ when $\Delta = 0$. Therefore one gets a double real root, meaning that there exists an intersection point of the sub- to super- and super- to subsonic flow patterns which is equivalent to the bifurcation point in the standard Parker solutions. The only difference is that, apart from the Mach number, all other physical quantities are discontinuous. The latter relation immediately gives $b = \pm 4\sqrt{C_*}$, so that at the critical point $\eta = \eta_*$ following two alternative equations are valid:

$$3\eta_*^4 \pm 4\sqrt{C_*}\eta_*^3 + C_*^2 = 0, \quad (30)$$

with the two possible double roots $\eta_* = \mp\sqrt{C_*}$, respectively. It is obvious that both roots satisfy the relation (17) as well.

Further, through the comparison of Eqs. (30) and (23) one can conclude that, accordingly, the algebraic equations having a family of solutions that correspond to the flows with patterns of (ξ, η) curves passing through the critical point $\eta = \eta_*$ read as:

$$3\eta^4 - 4 \left(1 \mp \left(\sqrt{C_*} \pm 1 \right) \frac{r}{r_*} \right) \eta^3 + C_*^2 = 0, \quad (31)$$

with

$$r_* = \mp \frac{4(\sqrt{C_*} \pm 1)}{D}. \quad (32)$$

In the case of $\eta_* = -\sqrt{C_*}$ ($b = 4\sqrt{C_*}$), the solution with the critical point $r = r_*$ is mathematically consistent. However, it gives negative η_* -s, i.e. it is requiring nonphysical imaginary sound speeds. Therefore, in this case, the part of the solution space given by the Eq. (31) does not have critical points where $M = 1$ in the domain $r > 0$ for any real value of the sound speed. Consequently, this version of the equation

does not generate transonic solutions and, thus, will not be considered further. Instead, we focus on the alternative case of Eq. (31) corresponding to case $\eta_* = \sqrt{C_*}$ ($b = -4\sqrt{C_*}$) and will explore the core physical content of the solutions it generates.

3.3 Sample solutions

In the present section, we perform an analysis of Eq. (31). Our aim is to plot typical flow patterns corresponding to sample sets of boundary conditions that give typical slow and fast wind patterns. In general, the detailed investigation of the available solution space requires a rather complex multi-variable parameter study in combination with the observable sets of synoptic maps and in-situ measurements. However, it should be taken into account that such a rigorous parameter study would require the inclusion of the effects of the energy sources and other non-adiabatic affects. While we are focusing here on a qualitative (semi-quantitative) demonstration of the principally novel space of the solutions on the bases of the adiabatic model, we just show two typical solutions for the slow and fast wind patterns with input parameters (boundary conditions at source surface and 1AU) that are in accordance with both the respective solar wind categorization schemes (e.g., see Xu & Borovsky 2015) and other general constraints on the boundary conditions known from the observational data (Matthaeus et al. 2006). These constraints form the general framework of relations between the parameter values that enables identification (distinction) of slow and fast solar wind patterns (in what follows we consider a mean slow wind case without subdivision of them into strahl reversal zone and streamer belt origin patterns as is done, for instance, by Xu & Borovsky (2015)). At any case, the categorization of the slow and fast solar winds requires that slow wind patterns have lower velocity and temperature and higher density values compared to the those of fast winds. The set of input and output parameters for both illustrative examples are given in Table 1. It is interesting to note that, brief parametric study of the solutions we build shows agreement and confirms observational evidence that the position of the sonic point is sensitive not only to the flow velocity but also to the temperature as well (Lotova & Obridko 2013).

The solution space we are investigating covers the values of $C_* \neq 1$ which implies nonzero values of parameter D , that itself maintains consistency and finiteness of the Eq. (22). In this case, a critical point exists (like in the isothermal case) where $M(r_*) = 1$ (denominator in Eq. (9) is zero). However, now $\eta(r_*) = \sqrt{C_*} \neq 1$ (nominator in Eq. (9) can be non-vanishing at the same point) meaning that the stationary solutions can sustain jumps in velocity, density and temperature radial profiles matching at the critical point, provided that there exists some external source of energy in that point supporting such a jump. We introduce one additional parameter - the altitude $r = r^{SS}$ (measured from the center of the Sun) of the source for a given stream and we use the superscript SS for all parameter values at this altitude. Its position is determined by the configuration of the magnetic field structures in the corona and the position of the critical point, thus it can change from region to region depending which type of flow pattern is considered. As was mentioned above, in a real situation this classification of

Table 1. The parameter values and boundary conditions.

Parameter	Slow wind	Fast wind
N^{SS} , cm ⁻³	$1.35 \cdot 10^{11}$	$8.83 \cdot 10^9$
N^{AU} , cm ⁻³	10.0	5.0
C_s^{SS} , km·s ⁻¹	240.00	240.00
C_s^{AU} , km·s ⁻¹	23.00	31.00
T^{SS} , K	$2.51 \cdot 10^6$	$2.51 \cdot 10^6$
T^{AU} , K	$2.31 \cdot 10^4$	$4.19 \cdot 10^4$
V^{SS} , km·s ⁻¹	$6.11 \cdot 10^{-4}$	$8.05 \cdot 10^{-3}$
V^{AU} , km·s ⁻¹	500.00	800
$Q_{C_s}^{SS}$, cm ⁴ s ⁻² g ^{-2/3}	$2.19 \cdot 10^{23}$	$1.35 \cdot 10^{24}$
$Q_{C_s}^{AU}$, cm ⁴ s ⁻² g ^{-2/3}	$1.14 \cdot 10^{28}$	$3.28 \cdot 10^{28}$
Q_β^{SS} , g s ⁻¹	$2.32 \cdot 10^{-11}$	$1.82 \cdot 10^{-11}$
Q_β^{AU} , g s ⁻¹	$2.32 \cdot 10^{-11}$	$1.82 \cdot 10^{-11}$
C_*^{SS}	$2.61 \cdot 10^{-6}$	$3.19 \cdot 10^{-5}$
C_*^{AU}	30.90	121.07
D^{SS} , cm ⁻¹	-0.57	-0.67
D^{AU} , cm ⁻¹	2.62	6.72
r^{SS} , R_\odot	1.68	1.61
r_* , R_\odot	6.97	5.95
F_e^{SS} , erg·cm ⁻² ·s ⁻¹	$-6.35 \cdot 10^3$	$-5.92 \cdot 10^3$
F_e^{AU} , erg·cm ⁻² ·s ⁻¹	$2.90 \cdot 10^4$	$5.95 \cdot 10^4$
ΔE_{tot} , erg·cm ⁻³	$3.00 \cdot 10^{-4}$	$2.15 \cdot 10^{-4}$
$ \Delta E_{tot}/E_1 $	1.08	1.22

patterns can be more complex unlike to the simple slow-fast wind we are adopting in this paper (such categorization can follow the one described in Xu & Borovsky (2015) or one related to corotating interaction regions). In both sample cases considered here, we presume that it is situated above the solar surface $r = r^{SS} > 1$.

We conditionally define the altitude of the source surface as the height at which the local temperature is approximately equal to 2.0 MK. We also set the values of the velocity, temperature and density at 1 AU which satisfies two conditions (we denote them with superscript AU): (i) the critical points of the sub- and supersonic parts of the flow patterns match in a single critical point thus enabling a smooth transonic transition of the Mach number and jumps in other quantities. (ii) the specific entropy, enclosed in the constant Q_{C_s} increases across the jump.

The result for the slow wind pattern is shown in Figure 1. In all panels, the blue and red colored curves correspond to the sub- and supersonic parts of the flow patterns, respectively. On the bottom x -axis of panels (a), (b) and (c) the radial distance is scaled by the solar radius R_\odot , while on the top horizontal axes of those panels it is normalized by the corresponding position of the critical point r_* (jump region). In panel (d) physical quantities are plotted against the local electron plasma frequency $f_{pe} = \sqrt{e^2 N / \pi m_e}$ (e is the elementary charge and m_e is the electron mass). In panel (a) the range of radial distances are taken between solar surface and 1 AU $R_\odot < r < 215R_\odot$ in order to demonstrate the position of the source surface $r = r^{SS}$ (which is marked by the thick vertical black slid line), while in the panels (b) and (c) this range is taken between source surface and 1 AU $r^{SS} < r < 215R_\odot$, as we assume that the lower boundary and corresponding conditions for the given wind stream is placed on the source surface and the curves below this radial distance are irrelevant for the current consideration.

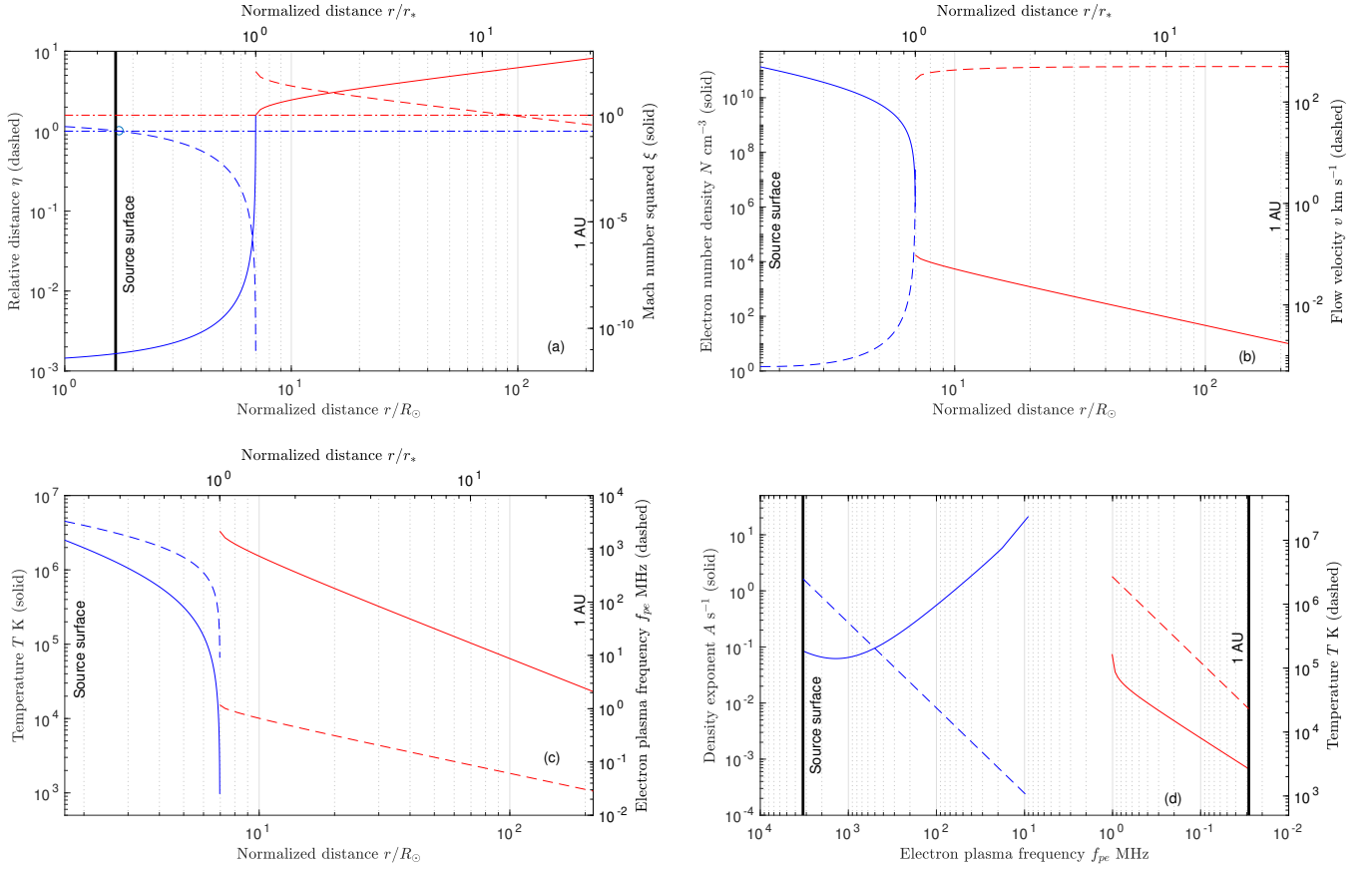


Figure 1. The slow solar wind pattern with parameters from the reference model (SWRM) for sub (blue curves) and supersonic (red curves) parts. Bottom x/R_\odot and top x/r_* (jump region) x-axes in panels (a), (b) and (c). The local electron plasma frequency f_{pe} on x-axis in panel (d). Panel (a): η (dashed curve, left y-axis) with horizontal blue dashed-dotted line indicating $\eta = 1$ level and cycles marking the places where the nominator of the Eq. (9) vanishes. Mach number squared $\xi = M^2$ (solid line, right y-axis). The red dashed-dotted horizontal line shows the level of $M = 1$. Thick vertical line - position of the source surface $r = r^{SS}$. panel (b) - Number density N (solid line, left y-axis) and flow velocity v (dashed line, right y-axis); panel (c) - Temperature T (solid line, left y-axis) and electron plasma frequency f_{pe} (dashed line, right y-axis); panel (d) - The number density exponent A and temperature T (dashed line, right y-axis) against the electron plasma frequency.

Further, in panel (a) we plot subsonic and supersonic curves of the relative distance η (dashed curve, the values are shown on the left y-axis). The horizontal blue dashed-dotted line indicates the reference line at $\eta = 1$ (the place where the nominator of the Eq. (9) vanishes). There are small circles marking the places of intersection of the curve of η with this line). The existence of such points constitutes an important difference to the standard Parker wind solution, which is always a monotonically growing function of r , while in our case the outflow velocity has a minimum on the subsonic and a maximum on the supersonic side. This means that the outflow velocity is bounded from both sides. The extremum on the subsonic side is not relevant in our examples as it is located below the source surface in each case. However, the velocity maximum on the supersonic side is very important as it means that with the set of parameters we use starting from a certain distance, which is at most of the order of 1 AU, the wind outflow should decelerate. This limits the applicability to a finite heliocentric distance range. The latter is, however, with up to 1 AU sufficiently large, and, thus, is more than needed to cover the innermost helio-

sphere for which we discuss the new solutions. We also plot in the same panel the Mach number squared $\xi = M^2$ (solid curve, the values are shown on the right y-axis). Again the red dashed-dotted horizontal line shows the level of $\xi = 1$. It is clearly seen that this line intersects with the curve of ξ at jump region $r = r_*$ where sub- and supersonic parts of the curve meet and, consequently, there is a smooth transition of Mach number without jump, as expected from our set up. In the other two panels we demonstrate corresponding radial profiles for other physical quantities within the domain $r^{SS} < r < 1$ AU in the following sequence: panel (b) - Number density N (solid curve, left y-axis) and flow velocity v (dashed curve, right y-axis); panel (c) - Temperature T (solid curve, left y-axis) and Electron plasma frequency f_{pe} (dashed curve, right y-axis); In panel (d) - The number density exponent A (solid blue curve, left y-axis, we give detailed outline of this parameter in section 4)

$$A \sim \frac{1}{N} \frac{dN}{dr}, \quad (33)$$

is reciprocal to the density scale height, and Temperature T (dashed line, right y-axis) are plotted vs. the electron plasma

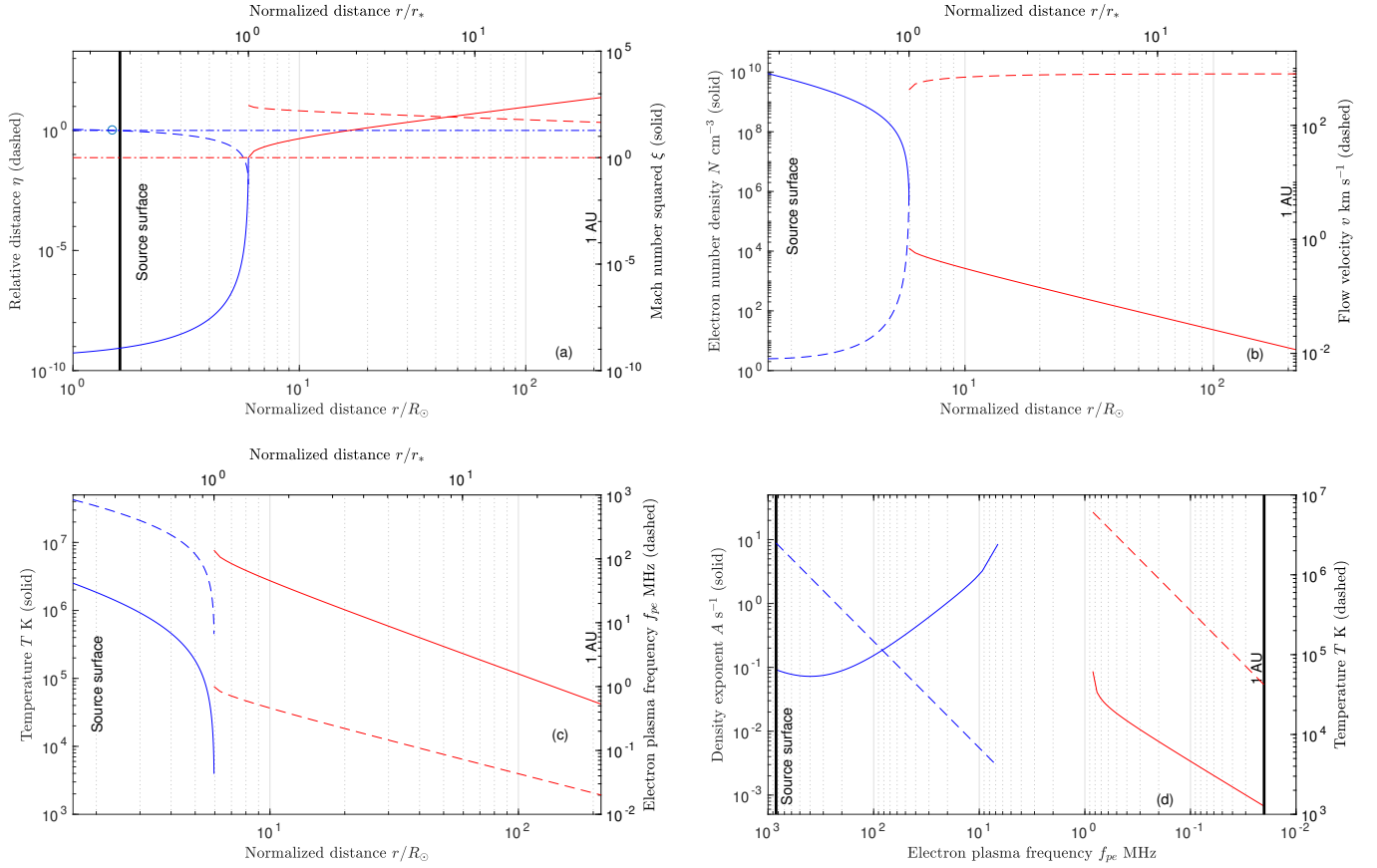


Figure 2. Same as in Figure 1 for fast wind typical pattern.

frequency (we discuss this below). In Figure 2 we plot the same physical quantities for the case of fast solar wind pattern with format and line styling identical to that of Figure 1.

Note that, while the velocity profiles shown in panel (b) of each figure look similar to classical Parker solutions (e.g., Parker 1958d), there is a principal difference: at the discontinuity at the sonic point, there is an infinite gradient, i.e. a jump, which is not present in Parker’s solution characterized by a smooth profile through the critical point.

It is important to note two aspects: (i) the shown examples of both slow and fast wind flow patterns demonstrate that the position of the critical points and entire shape of the patterns are extremely sensitive to the temperature (Mach number) values and its profiles on both sides of the flow. (ii) The curves plotted in the panel (d) of both figures are closely related with the contemporary radio observations. The outline of the links with these observations will be the matter of our forthcoming work, to be published elsewhere.

3.4 Connection to observations

The most insightful observational data are expected from the recently launched Parker Solar Probe (Fox et al. 2016) and Solar Orbiter (Müller et al. 2013) missions, which will probe the solar wind source region and may discover the type of flow patterns we model here analytically. With the advance of these missions and the increasing amount of in-situ data one could address the specific task to check for

quasistationary flow patterns similar to those derived in the present study.

In the meantime, until a sufficient amount of these data will be available, we can look for possible indirect manifestations of the discontinuities in flow velocity and density in other observations. For instance, solar radio emissions allow one to infer information on the density, temperature and related profiles in the solar environment. The source of information consists of the characteristic spectral properties of the different types of radio bursts in dynamic radio spectra. Such spectra cover ranges of radio frequencies starting from several hundreds of MHz (high density regions close to the Sun) down to tens of kHz (interplanetary space, close to the Earth).

We demonstrate in Figures (1)-(2) (panels (c) and (d)) the ranges of the local electron plasma frequency f_{pe} which, in general, constitutes a key determining factor for the frequency spectra of the radio waves emitted by the solar wind as well as coronal plasma and transmitted to an observer located at 1 AU. Evidently, the ranges of f_{pe} reproduced by our solar wind model are in good agreement with observed spectra, (e.g. see Chernov 2011).

The drift of the intensity peaks related to type III radio bursts enables one to determine the mean inverted density scale-height A that is also plotted as solid lines in panels (d) of the above two figures. In addition, it is also of interest to note that $T - f_{pe}$ diagrams (dashed lines in panels (d)) are also useful for an analysis of the model by matching

it with the temperature and density profiles inferred from the radio observations. This is one of the directions where the results of our solar wind solutions can aim at. A similar model-dependent analysis for the case of the isothermal solar wind has been reported earlier by Mann et al. (1999), where the authors considered the particular case with a uniform temperature.

An important issue is how the theoretically predicted jump regions could be manifested in the dynamic radio spectra. In general, there are few observational evidence of ‘atypical’ properties of radio bursts that can appear at different values of the emitted frequency. Here we provide an example out of them. It is intuitively evident from the obtained density profiles in the Figures (1)-(2), that the jump regions can be sources of an rather unusual behaviour of the frequency drift rates in Type III radio bursts (in some cases, an infinite or even changing sign drift may be observable). Observations of solar radio emission in the decameter range revealed that occasionally there are bursts of type III that differ from ordinary bursts of that type, particularly in the drift velocity. Typical decameter type III bursts have negative drift velocities, the magnitude of which varies within 2-4 MHz s⁻¹ (MelNik et al. 2005), but type III bursts with high frequency drift rates up to 42 MHz s⁻¹ were recorded (MelNik et al. 2008) as well.

As an example, the unusual type III bursts having a sharp, i.e. abrupt frequency drift breaking (Brazhenko et al. 2015; Melnik et al. 2014) are addressed here (Figure 3). In some cases, this break occurs from the high frequency side, and in some cases from the low frequency side. Such bursts can be generated from fast electrons moving through the coronal plasma, either before the discontinuity in the density (breaking/disappearance from the low frequency side) or behind it, when the sudden burst occurs on the high-frequency side.

Naturally, the development of a novel framework for the interpretation of the different types of radio bursts on the basis of the novel analytic solutions for solar wind patterns obtained in this paper needs a more rigorous separate formulation and this will be carried out in more detail elsewhere. We presented here just a single illustrative example.

3.5 Physical conditions for the new class of solutions

Appearance of the derived non-smooth solutions requires a certain framework for the constraints making them realizable in real physical situations. One important issue is the second law of thermodynamics that demands that the entropy must increase along the streamlines or, at least, stays constant in isentropic flow. A second one is the distinction of these non-smooth solutions from classic hydrodynamic shock solutions.

3.5.1 Classical shocks

In the classic case we have a supersonic flow upstream of a shock that undergoes a strong deceleration to the subsonic state downstream. The jump occurs in a thin shock region where it is assumed that the particle or wave-particle collision-related dissipation (microscopic transport)

processes prevail and act during the mean collision time on mean-free-path scales. These effects are implicitly presumed in the physical description although they are not explicitly included in the governing hydrodynamic equations. The physics is that the kinetic energy of upstream supersonic flow is strongly dissipated in the shock region resulting in increase of the entropy across the shock. This process satisfies the requirement of the second law and imposes the irreversible nature of the flow. As is known from the classic theory of shocks, the jump of physical quantities is sudden because the fluid elements being far upstream do not feel the presence ahead of the region with enhanced collisions. This is due to the supersonic velocity of the ambient flow preventing acoustic waves propagation upstream, as transmitters of the information about the pressure and density changes in the system. Therefore, the state of the flow suddenly adapts to the new physical conditions ahead manifested in form of the shock jump. In the SW context such classic shock solutions have been derived for the flows with multiple critical points (Leer & Holzer 1990; Holzer 1977).

3.5.2 The new discontinuities

In the new model the configuration of the flow and physics governing its radial structure is completely different from classical shocks: the upstream flow is subsonic and there is no kinetic energy embedded in the flow that could be dissipated. Instead the flow is accelerated to the supersonic state formed in the downstream region. There are two alternatives for explanation.

The first one is to consider the dynamics opposite to the one observed in the classic case. If we allow the entropy to decrease along the streamlines, then we obtain a picture which is forbidden by the second law, unless we take into account a more global thermodynamic process enabling local entropy dissipation or transport to neighboring regions. Mathematically such thermodynamical nonequilibrium process should be manifest in the form of additional source terms in the original system of equations (1)-(3). However, we do not cover this possibility with the current study.

The second possibility is to assume that the entropy is indeed increasing across the jump at the critical point. Since such process can in our case not be sustained at the expense of ambient flow bulk kinetic energy, some additional physical process, acting only within the jump region of the collisionless plasma flow, is needed that could be responsible for such a growth of the entropy.

Among other candidate scenarios, one can draw the following possible heuristics of the process. Let us imagine that, on the upstream side as the flow is accelerated radially the density drops because of radial expansion and mass continuity. This means that the plasma is adiabatically expanding and cooling, so that in a given fluid element the temperature and, thus, the sound speed $C_s(r)$ become lower upon approaching the critical point where $M = 1$. At the same time the ambient flow velocity approaches the sonic value, i.e. $v(r) = C_s(r) - \varepsilon(r)$, with $\varepsilon(r)$ denoting velocities much lower than the sound speed. To deliver the information about the changing physical conditions to regions far upstream backward propagating sound waves are needed. However, their effective phase velocity in the sunward direction $\varepsilon(r)$ is very low as the flow velocity is almost sonic.

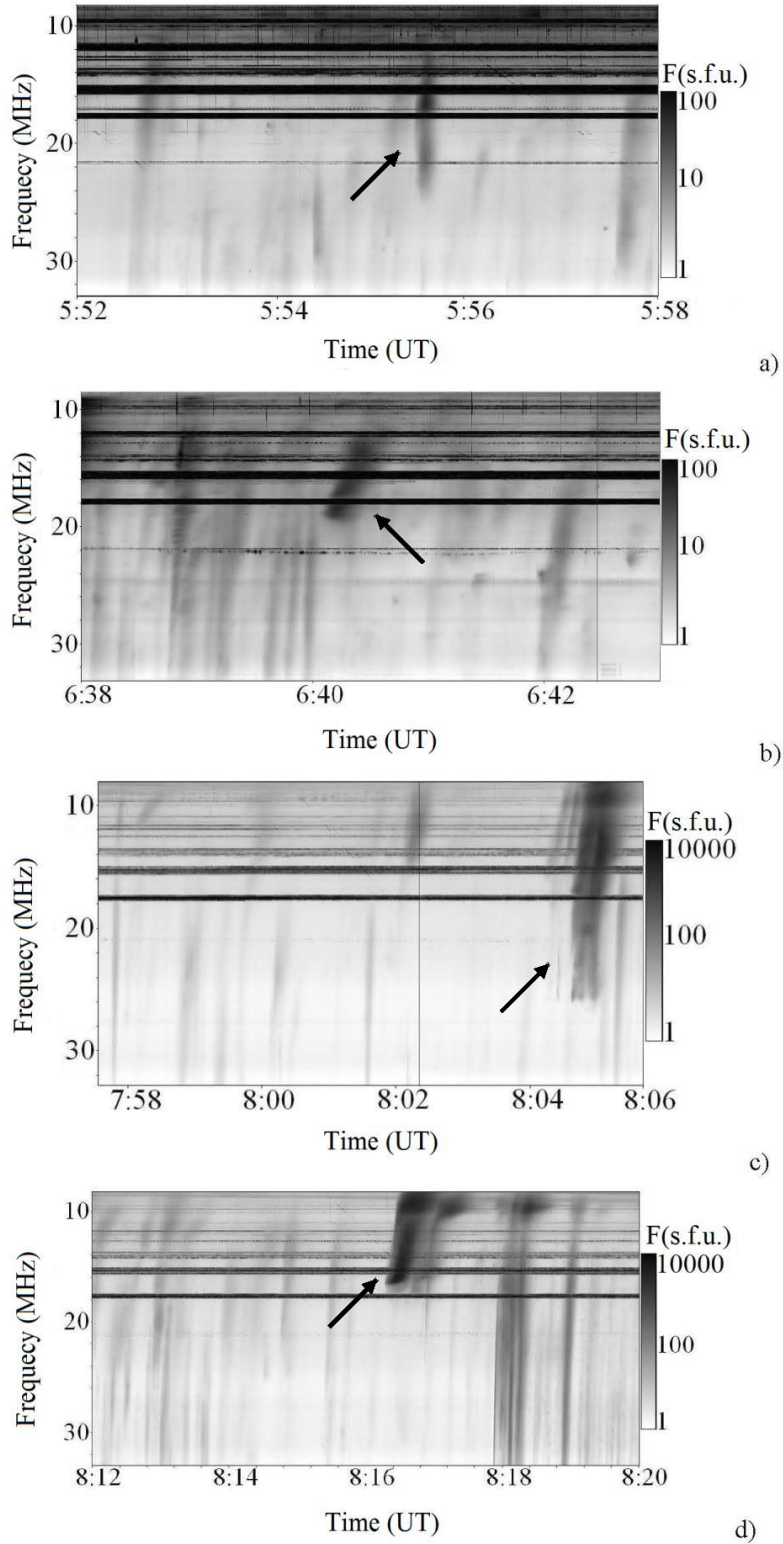


Figure 3. Dynamic radio spectra of the caterpillar bursts observed by URAN-2 radio telescope (Brazhenko et al. 2015; Melnik et al. 2014). The sample bursts are marked by arrows.

Therefore, similarly to the classic shock case, the regions far upstream are not aware of the presence of changed physical conditions ahead. The effect is similar but the physical reasoning behind the process is different. Regardless of the nature of this reasoning the results is that the system is forced to adapt to suddenly appearing physical conditions at the critical point, providing the possibility of non-smooth jumps as described above.

3.5.3 An estimate of required energy

It is important to estimate the contribution of the external source of energy that can supply the jump of the flow total energy and its flux densities. For this it should be noted that from Eqs.(4)-(6) it can be readily derived the conservation law for the total energy flux density F_e :

$$\frac{d}{dr} \left[\rho v r^2 \left(h + \frac{v^2}{2} \right) \right] = 0 \quad (34)$$

where

$$h = -\frac{GM_\odot}{r} + \frac{C_s^2}{\alpha - 1}.$$

The constant values of the total energy flux density on upstream and downstream sides differ from each other (as is shown in Table 1 for fast and slow wind). Therefore, The external source of energy acting in the vicinity of the critical point must produce an extra energy flux to sustain the necessary jump. The key aspect is that the total energy flux should be balanced in the critical point $r = r_*$, so that:

$$v_1 E_1 + C_{F_e} = v_2 E_2, \quad (35)$$

where

$$E_1 = \rho_1 \left[\frac{C_{s1}^2 (\alpha + 1)}{2(\alpha - 1)} - \frac{GM_\odot}{r_*} \right], \quad (36)$$

and

$$E_2 = \rho_2 \left[\frac{C_{s2}^2 (\alpha + 1)}{2(\alpha - 1)} - \frac{GM_\odot}{r_*} \right], \quad (37)$$

are the total energy densities in the critical point on the upstream and downstream side, respectively, and the constant C_{F_e} contains the information on the external source of energy (see further description) that supports a transition from an upstream subsonic to a downstream supersonic state. When such source of energy is absent, then the non-smooth, discontinuous flow patterns derived within our framework is not realizable and in that case solely the classic smooth Parker type transonic patterns are possible. The definitions (36)-(37) can be employed to estimate the amount of total energy density that should be generated at the critical point by the external source relative to upstream total energy density (at the same point), to provide a jump-like transition from sub- to supersonic state of the flow:

$$\left| \frac{\Delta E_{Tot}}{E_1} \right| = \left| \frac{E_2}{E_1} - 1 \right|, \quad (38)$$

The values of this relative total energy density difference are given in Table 1, accordingly. It is interesting to note that ΔE_{Tot} for both slow and fast solar wind patterns is by several orders of magnitude smaller than the amount of total energy released by any standard flare event (e.g., Fleishman

et al. 2015; Ellison 1963), even taking into account the radial expansion in the upward direction. This fact makes the scenarios described here easily sustainable by any reconnection type explosive event or their combinations in the solar corona.

In our case we observe that the temperature and density gradients become very large at the sonic point, therefore this region can effectively play the role of a wave reflector and, thus, serve as a source of backward propagating acoustic waves (e.g., see Brekhovskikh & Godin 1990, 1999). Consideration of solely longitudinal compressional acoustic waves is justified by two reasons: (i) we consider here a purely radial hydrodynamic model omitting all magnetic effects; (ii) if we would take into account the presence of the incompressible Alfvén waves they propagate much faster than with sound speed, i.e. $V_A \gg C_s$, in the low beta plasma and, thus, propagate out of the jump region quickly and can not contribute efficiently to the local rapid heating and entropy generation in the vicinity of the sonic point.

For case (i), i.e. the reflection of acoustic waves, we can, e.g., follow the theory by Lekner (1990b) and Lekner (1990a) in combination with the method used by Mishonov et al. (2007). According to these authors, the heating power is given by a frequency integral of the damping rate τ_d^{-1} (expressed via the dissipation time scale) and the spectral density $\Phi(f)$:

$$Q_{diss} = \frac{\rho}{2} \int_{f_{min}}^{f_{max}} \frac{\Phi(f)}{\tau_d} df = \Delta E_{tot} \quad (39)$$

where f_{min} and f_{max} represent the boundary frequencies of the wave spectrum.

At this point it is important to clarify from where the mentioned longitudinal (ion-) acoustic wave spectrum can arise and whether such spectrum can be sustained by the system we consider. Evidently, the ambient flow can take part in the formation of the spectrum of waves, but w.r.t. to the above modeling, we are interested in the situation that it is not the primary source of the wave energy. The latter is treated such that an external source is needed. The presence of compressional longitudinal waves in such a medium is easily justified, because once the Mach number exceeds the value 0.3, then the flow in principle can not be treated as incompressible (e.g., Gatski & Bonnet 2013). Thus, compressional disturbances may become abundant in the flow provided that corresponding sources exist. This scenario is further supported by the fact that both density and temperature decrease adiabatically in the subsonic part of the flow (see our sample solutions), thereby providing a gradual growth of the compressibility coefficient $1/\rho C_s^2$ as the flow approaches the critical point.

Consequently, upon assuming that wave sources are able to excite the acoustic modes directly or indirectly via conversion of other wave modes, the system can sustain a certain spectrum of such waves. The direct sources include, e.g., magnetic reconnection related eruptive events or the existence of magnetic clouds and density inhomogeneities that play the role of obstacles for local jet-like flows providing excitation of the waves in the wake behind the obstacle. The indirect sources comprise, amongst other processes, weekly (almost non-) dissipative Alfvén waves transporting the wave energy to the vicinity of the critical point where they are converted into compressional waves (e.g. Jiling 1999; Malik

et al. 2007). The other mechanisms of the mode conversion can be also active, e.g. by the nonuniform magnetic field and density (resonant absorption), or shear flows (nonmodal wave conversion). The main point is here that these alternatives, while operating in different regions of the solar wind source region, they do so locally. Such a local nature of the flow pattern formation is vividly justified by the most recent observations by the Parker Solar Probe mission that already revealed a complex structure of the solar wind (Bale et al. 2019; Kasper et al. 2019).

It is known that when the electron and ion temperatures are equal $T_e \approx T_i$, then the ion-acoustic waves undergo strong Landau damping and their phase velocity $C_{si}^2 = k_B T_e / m_i$ is close to the ion thermal velocity $k_B T_i / m_i$ where the damping rate is maximum. Hence, the relation between the propagation and damping time scales should accurately be taken into account. The following scenarios maybe realized locally in the source region: (i) When $T_e \neq T_i$ it is expected that the ion-acoustic waves have a finite lifetime and are able to propagate towards the critical point, get reflected and damp; (ii) When the Landau damping is strong ($T_e \approx T_i$) the waves get dissipated within a wave period. To make this process efficient for the temperature jump at the critical point, the sources must be situated in the immediate vicinity of or even within the critical point.

3.5.4 An estimate of the intensity of reflected waves

The goal is estimating the wave energy needed to sustain the sharp temperature jump in the total energy density ΔE_{tot} . Following Mishonov et al. (2007) the damping rate can be expressed as $\tau_d^{-1} = \nu_{tot} k^2$ with the total 'viscosity' ν_{tot} and the wave number k , which for the reflected waves with phase speed ε and frequency f is $k = 2\pi f / \varepsilon$. The total viscosity may include three types of transport processes, i.e., $\nu_{tot} = \nu_k + \nu_{wp} + \nu_{ww}$, where the three terms denote the kinematic, wave-particle and wave-wave 'viscosities', respectively. While ν_k can arise locally due to particle collisions, ν_{wp} and ν_{ww} can be due to the Landau damping of the waves and wave turbulence, respectively. Upon considering a power law spectrum $\Phi(f) = K f^{-x}$ for the reflected waves, we obtain

$$\frac{K \rho \varepsilon^2}{8\pi^2 \nu_{Tot}(x+1)} \left(f_{min}^{-(x+1)} - f_{max}^{-(x+1)} \right) = \Delta E_{tot} \quad (40)$$

From this equation one can, for a given temperature jump ΔT , estimate the constant K as a measure of the reflected wave field intensity.

So, in general terms, instead of the kinetic energy of the flow, the dissipation of acoustic waves can be the source of the entropy and heat, i.e. particle acceleration in the jump region. The produced heat leads to a drastic increase of the temperature and to local non-adiabatic expansion of the plasma, resulting in the discontinuous rarefaction jump in density. This scenario is consistent with the second law and it is what we observe in our example solutions.

4 SUMMARY AND CONCLUSIONS

In this paper we reported on the results of a new, rather simplified, one-dimensional quasi-polytropic radial solar wind

expansion model, with particular emphasis on the case of an adiabatic index $\alpha = 5/3$. We demonstrated that, in this case, the governing equations reduce to a specific form generating exact analytic solutions for the solar wind patterns. The solutions respect both mathematical and physical consistency conditions and thus could be used for the numerical modelling of the solar wind using also observed solar synoptic maps for better prediction of the space weather conditions.

The analytic framework derived in this study provides a substantial novel class of solutions, which have not been addressed in any previous model of the solar wind. The novelty in the solution space occurs as a result of a local heating enabling (provided that Mach number is still continuous) jumps of the density, velocity, and temperature at the sonic point. Rather than modelling such heating explicitly, it is implicit in the construction of the solution by matching appropriate sub- and supersonic branches, this way allowing for a simplified modelling. The similar framework can be used not only for the large radially extended solar wind patterns, but also for the modeling of small-scale flows in solar corona e.g. coronal jets (see, Bagashvili et al. 2018, and references therein).

There are other immediate extensions of this study. For instance the generalization for the case of arbitrary value of the polytropic index, also including different types of sources of the heat and acceleration of the solar wind plasma. The model can be used for the construction of more complexly structured multidimensional analytical solar and stellar wind patterns (see, e.g. Sauty et al. 1998, 2002; Tsinganos 2007, and references therein). Thus, the theoretical model demonstrated in this manuscript could be considered as paving the way towards a development of an increased variety of solar wind models useful for space weather and/or heliospheric studies.

ACKNOWLEDGEMENTS

The work was supported by Shota Rustaveli National Science Foundation grants DI-2016-52, FR17-609 and partially by European Commission FP7-PEOPLE-2010-IRSES-269299 project - SOLSPANET. The work of G.D. has been realized within the framework of Shota Rustaveli National Science Foundation PHD student's research (individual) grant DO/138/6-310/14 and grant for young scientists for scientific research internship abroad IG/47/1/16. Work of B.M.S. was supported by the Austrian Fonds zur Forderung der wissenschaftlichen Forschung (FWF) under projects P25640-N27, S11606-N16. B.M.S. and H. Fichtner acknowledge support from the German Research Foundation (DFG) via the collaboration grant FI 706/25-1. Work of B.M.S. and H. Foysi was partially supported by the DFG collaboration grant FO 674/12-1. The work of T.V.Z. was supported by FWF under projects P25640-N27 and P30695-N27. M.L.K. additionally acknowledges the support by FWF project I2939-N27 and the grant No. 18-12-00080 of the Russian Science Foundation, as well as the project "Study of stars with exoplanets" within the grant No.075-15-2019-1875 from the government of Russian Federation. S.P. was supported by the projects GOA/2015-014 (KU Leuven), G.0A23.16N (FWO-Vlaanderen) and C 90347 (ESA Prodex). We are thankful to the anonymous reviewer for

constructive and valuable remarks on our manuscript that led to significant improvement of the content.

REFERENCES

- Bagashvili S. R., Shergelashvili B. M., Japaridze D. R., Kukhianidze V., Poedts S., Zaqarashvili T. V., Khodachenko M. L., De Causmaecker P., 2018, *ApJ*, **855**, L21
- Bale S., et al., 2019, *Nature*, 576
- Brazhenko A. I., Melnik V. M., Frantsuzenko A. V., Rucker H. O., Panchenko M., 2015, *Russian Radio Physics and Radio Astronomy*, **20**, 10
- Brekhovskikh L. M., Godin O.-A., 1990, *Acoustics of Layered Media I: Plane and Quasi-Plane Waves*. Springer Verlag, Berlin
- Brekhovskikh L. M., Godin O.-A., 1999, *Acoustics of Layered Media II: Point Sources and Bounded Beams*. Springer Verlag, Berlin
- Chernov G. P., ed. 2011, *Fine Structure of Solar Radio Bursts Astrophysics and Space Science Library Vol. 375*, doi:10.1007/978-3-642-20015-1.
- Cranmer S. R., Winebarger A. R., 2019, *ARA&A*, **57**, 157
- Echim M. M., Lemaire J., Lie-Svendsen Ø., 2011, *Surveys in Geophysics*, **32**, 1
- Ellison M. A., 1963, *QJRAS*, **4**, 62
- Feldman U., Landi E., Schwadron N. A., 2005, *Journal of Geophysical Research (Space Physics)*, **110**, A07109
- Fleishman G. D., Nita G. M., Gary D. E., 2015, *ApJ*, **802**, 122
- Fox N. J., et al., 2016, *Space Sci. Rev.*, **204**, 7
- Gatski T. B., Bonnet J.-P., 2013, *Compressibility, Turbulence and High Speed Flow (2nd edition)*. Academic press in an imprint of Elsevier
- Holzer T. E., 1977, *J. Geophys. Res.*, **82**, 23
- Jacobs C., Poedts S., 2011, *Advances in Space Research*, **48**, 1958
- Jiling H., 1999, *Sol. Phys.*, **185**, 391
- Kasper J. C., et al., 2019, *Nature*, 576, 228
- Leer E., Holzer T. E., 1990, *ApJ*, **358**, 680
- Lekner J., 1990a, *Acoustical Society of America Journal*, **87**, 2325
- Lekner J., 1990b, *Acoustical Society of America Journal*, **88**, 2876
- Lotova N. A., Obridko V. N., 2013, *Astronomy Letters*, **39**, 474
- Malik M., Sharma R. P., Singh H. D., 2007, *Sol. Phys.*, **241**, 317
- Mann G., Jansen F., MacDowall R. J., Kaiser M. L., Stone R. G., 1999, *A&A*, **348**, 614
- Matthaeus W. H., Elliott H. A., McComas D. J., 2006, *Journal of Geophysical Research (Space Physics)*, **111**, A10103
- MelNik V. N., Konovalenko A. A., Abranin E. P., Dorovskyy V. V., Stanislavsky A. A., Rucker H. O., Lecacheux A., 2005, *Astronomical and Astrophysical Transactions*, **24**, 391
- MelNik V. N., et al., 2008, *Sol. Phys.*, **250**, 133
- Melnik V. N., Brazhenko A. I., Konovalenko A. A., Rucker H. O., Frantsuzenko A. V., Dorovskyy V. V., Panchenko M., Stanislavskyy A. A., 2014, *Sol. Phys.*, **289**, 263
- Mishonov T. M., Stoev M. V., Maneva Y. G., 2007, *Theory of heating of hot magnetized plasma by Alfvén waves. Application for solar corona (arXiv:astro-ph/0701554)*
- Müller D., Marsden R. G., St. Cyr O. C., Gilbert H. R., 2013, *Sol. Phys.*, **285**, 25
- Odstroil D., 2003, *Advances in Space Research*, **32**, 497
- Parker E. N., 1958a, *Physics of Fluids*, **1**, 171
- Parker E. N., 1958b, *Physical Review*, **109**, 1874
- Parker E. N., 1958c, *Physical Review*, **110**, 1445
- Parker E. N., 1958d, *ApJ*, **128**, 664
- Parker E. N., 1959a, *ApJ*, **129**, 217
- Parker E. N., 1959b, *ApJ*, **129**, 860
- Parker E. N., 1965a, *Space Sci. Rev.*, **4**, 666
- Parker E. N., 1965b, *Planet. Space Sci.*, **13**, 9
- Pomoell J., Poedts S., 2018, *Journal of Space Weather and Space Climate*, **8**, A35
- Sauty C., Tsinganos K., Trussoni E., 1998, *Ap&SS*, **261**, 151
- Sauty C., Trussoni E., Tsinganos K., 2002, *A&A*, **389**, 1068
- Shergelashvili B. M., Fichtner H., 2012, *ApJ*, **752**, 142
- Shergelashvili B. M., Poedts S., Pataraya A. D., 2006, *ApJ*, **642**, L73
- Shergelashvili B. M., Maes C., Poedts S., Zaqarashvili T. V., 2007, *Phys. Rev. E*, **76**, 046404
- Summers D., 1982, *ApJ*, **257**, 881
- Tsinganos K., 1996, *Advances in Space Research*, **17**, 65
- Tsinganos K., 2007, *Theory of MHD Jets and Outflows*, in *Lecture Notes in Physics*, Vol. 723. Berlin Springer Verlag, p. 117
- Vainio R., Laitinen T., Fichtner H., 2003, *A&A*, **407**, 713
- Xu F., Borovsky J. E., 2015, *Journal of Geophysical Research (Space Physics)*, **120**, 70
- van der Holst B., Sokolov I. V., Meng X., Jin M., Manchester IV W. B., Tóth G., Gombosi T. I., 2014, *ApJ*, **782**, 81

This paper has been typeset from a $\text{\TeX}/\text{\LaTeX}$ file prepared by the author.